

Development and validation of a full polarimetric radar simulator

Clotilde Augros^{*1}, Pierre Tabary¹, Olivier Caumont², and Véronique Ducrocq²

¹DSO/CMR, Météo-France, Toulouse, France

²CNRM/GAME (Météo-France, CNRS), Toulouse, France

1 INTRODUCTION

Significant efforts have been done these last years to upgrade and densify the French operational radar network (called ARAMIS). In particular, polarimetry is now considered the new operational standard and 17 (12 C-band, 2 S-band and 3 X-band) out of 27 radars are polarimetric, as shown in Figure 1. The radar network will be fully polarimetric by 2020.

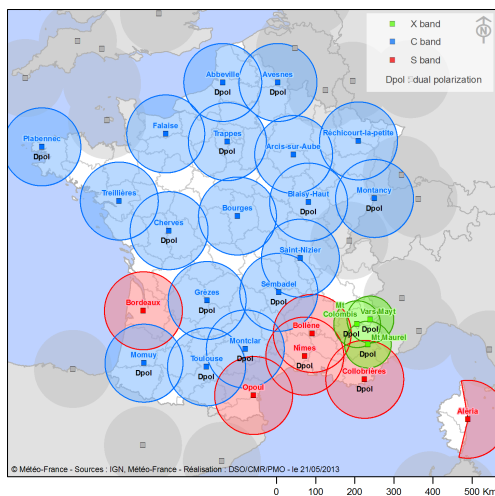


Figure 1: The French radar network in 2013

Continuous work has therefore been done to understand, monitor and exploit the polarimetric variables for operational products. This led to a first operational version of a polarimetric processing chain, including precipitation-induced attenuation correction, non meteorological echo identification and data quality monitoring (Figueras i Ventura et al., 2012). Dual-polarimetric quantitative precipitation algorithms were also developed (Figueras i Ventura and Tabary, 2013; Kabeche et al.,

2012) as well as a new hydrometeors classification scheme for S, C and X band radars (Al-Sakka et al., 2013).

While quantitative precipitation estimations are greatly improved by the use of polarimetric data, the polarimetric variables could also be used for data assimilation and model verification in convection-resolving Numerical Weather Prediction (NWP) models as they provide unique information on the microphysical properties of hydrometeors. Up to now, only reflectivity (Caumont et al., 2010) and radial velocity (Montmerle and Faciani, 2009), among radar variables, are assimilated in the French convective-scale operational model Application of Research to Operations at Mesoscale (AROME) (Seity et al., 2011). But as more and more radars from the French network include dual-pol capabilities, the use of dual-pol radar data in AROME needs to be investigated.

In order to examine how to best use dual-pol data for assimilation in convection-resolving models, direct comparisons between measured dual-pol data and numerically modeled data need first to be conducted. For this purpose, a simulator for polarimetric radar variables (such as e. g. Jung et al. (2008), Pfeifer et al. (2008), Ryzhkov et al. (2011)) has been developed. The simulator calculates polarimetric radar variables from the prognostic output of the research nonhydrostatic mesoscale atmospheric model (Meso-NH Lafore et al. (1998)).

A detailed description of the simulator is given in section 2. The simulated polarimetric variables were compared to observations on a case with an intense bow echo. The case study and the simulation design are detailed in section 3 while the results are outlined in section 4.

^{*}Corresponding author address: Clotilde Augros, Météo-France, DSO/CMR/DEP, 31 057 Toulouse CEDEX 1, France; e-mail: clotilde.augros@meteo.fr.

2 THE POLARIMETRIC RADAR SIMULATOR

The polarimetric radar simulator is an upgraded version of the radar simulator developed by Caumont et al. (2006). It calculates the radar polarimetric observables from the prognostic output of the Meso-NH model. Electromagnetic wave propagation and scattering at S, C, and X bands are simulated. Beam propagation effects are considered, including (differential) attenuation and phase shift, beam bending, and beam broadening. The range-dependent noise level is also simulated. Meso-NH model is first briefly described in subsection 2.1. The different scattering methods are then exposed in subsection 2.2. The hydrometeor characteristics are discussed in subsection 2.3 and finally, the calculation of the polarimetric variables is detailed in subsection 2.4.

2.1 Meso-NH model

The polarimetric radar simulator is developed inside the postprocessing software of Meso-NH model, the characteristics of which are very close to those of the operational convective scale NWP system AROME. In particular, Meso-NH and AROME models use the same one-moment bulk microphysical scheme named ICE3 (Pinty and Jabouille, 1998) governing the equations of the six following water species: vapor, cloud water, rain, graupel, snow, and pristine ice. The diameter spectrum of each water species is assumed to follow a generalized Gamma distribution (simplified in a more classical exponential distribution for precipitating species). Power-law relationships are used to link the mass and the terminal speed velocity to the particle diameters. The simulator is fully consistent with the microphysical parameterizations of MesoNH model.

2.2 Scattering

In the polarimetric radar simulator, scattering by rain, graupel, snow and pristine ice particles only is simulated. Scattering by cloud vapor is neglected. The radar simulator from Caumont et al. (2006) offers the possibility to choose among Rayleigh, Rayleigh–Gans, Mie, or T-matrix (Mishchenko and Travis, 1994) scattering methods. In the polarimetric radar simulator, Rayleigh scattering method is chosen for pristine ice particles, which are considered to be spherical, whereas T-matrix method is selected for rain, snow and graupel particles that are simulated as spheroids. To ensure optimum efficiency, T-matrix lookup tables containing the scattering coefficients were computed in advance, for a range of hydrometeor contents, temperatures, elevation angles and wavelengths for each hydrometeor specie.

2.3 Hydrometeor characteristics

2.3.1 Dielectric constant

The dielectric constant of all species are calculated in the same way as in Caumont et al. (2006). The dielectric function of rain is taken from Liebe et al. (1991). Snow and graupel above the melting level are considered to be made of pure ice and their dielectric function is calculated with the model of Hufford (1991), like for pristine ice. The equivalent diameter of snow and graupel above the melting level is the one of a sphere of pure ice that would have the same mass. For water-coated graupel (below the melting level), which is made of ice, water, and air, the diameter is the one of an equivalent-mass sphere made of 14% water and 86% ice as spheroidal inclusions. The corresponding dielectric function is computed following Bohren and Battan (1982).

2.3.2 Shape

Rain particles are simulated as spheroids. Different formulations of aspect ratio are implemented in the radar simulator. For the polarimetric radar simulator, the aspect ratio is calculated following Brandes et al. (2002), as done in the polarimetric radar simulator from Ryzhkov et al. (2011). Snow and graupel particles are also simulated as spheroids. A fixed axis ratio of 0.75 is used for snow and for graupel (as in Jung et al. (2008)). Pristine ice particles are simulated as spheres.

2.3.3 Oscillation

We assume that the hydrometeors with oblate shapes are characterized by Gaussian distribution of orientations with zero mean canting angle. The width of canting angle distribution is assumed to be 10° for rain, 20° for snow and 40° for graupel (as in the simulator from Ryzhkov et al. (2011)). These values were chosen arbitrarily following the literature but sensitivity studies will be carried out in the future in order to establish what values fit best our data.

2.4 Calculation of the polarimetric variables

Rayleigh or T-matrix scattering methods provide the back and forward scattering coefficients $S_{hh, vv}^b(D)$ on the horizontal and vertical polarizations, for a single hydrometeor with a given diameter D . The polarimetric variables are then calculated by integrating the scattering coefficients over the drop size distribution $N_x(D)$ of each specie (x). The formulas for the horizontal reflectivity Z_{hh} , the differential reflectivity Z_{dr} , the specific differential phase K_{dp} , the differential phase ϕ_{dp} and the copolar correlation coefficient ρ_{hv} are given in equations 1 to 5 where λ is the radar wavelength (m), $|K_w|^2$ is the dielectric factor, D is the diameter (m).

$$Z_{hh,vv} = 10 \log_{10} \left(10^{18} \frac{4\pi\lambda^4}{\pi^5 |K_w|^2} \sum_{x=1}^n \int_{D_{min}}^{D_{max}} |S_{hh,vv_x}^b(D)|^2 N_x(D) dD \right) \quad (dBZ) \quad (1)$$

$$Z_{dr} = Z_{hh} - Z_{vv} \quad (dB) \quad (2)$$

$$K_{dp} = 10^3 \lambda \frac{180}{\pi} \sum_{x=1}^n \int_{D_{min}}^{D_{max}} \text{Re}(S_{hh}^f - S_{vv}^f) N_x(D) dD \quad (^\circ km^{-1}) \quad (3)$$

$$\phi_{dp} = 2 \int_0^{r_{max}} K_{dp}(r) dr \quad (^\circ) \quad (4)$$

$$\rho_{hv} = \frac{\left| \sum_{x=1}^n \int_{D_{min}}^{D_{max}} S_{hh_x}^b * (D) S_{vv_x}^b(D) N_x(D) dD \right|}{\sqrt{\sum_{x=1}^n \int_{D_{min}}^{D_{max}} |S_{hh_x}^b(D)|^2 N_x(D) dD \sum_{x=1}^n \int_{D_{min}}^{D_{max}} |S_{vv_x}^b(D)|^2 N_x(D) dD}} \quad (-) \quad (5)$$

3 CASE STUDY AND SIMULATION DESIGN

(2013).

3.1 Meteorological situation

A bow echo case on 24 September 2012 in south-eastern France was chosen for the simulation. This case is particularly interesting as it is included in HyMeX (Hydrological cycle in Mediterranean Experiment, Ducrocq (2013) and Drobinsky (2013)) measurement campaign, during which supplementary observations were available (radars, radiosoundings, aircraft data) in the south-east of France. This case is identified as IOP6.

On this day, a trough extended from Iceland to Brittany and induced a south-westerly flow in south-east France and high level cold advection. At 00 UTC, a convective line extended from north Spain to center France as shown on Figure 2 (a). While moving eastwards, this line merged with orographic precipitation on Cévennes, and the whole system became more and more organized until forming a bow echo, clearly visible at 03 UTC. After 06 UTC the system moved eastwards and its activity decreased. More detail on this case are given in Ducrocq

3.2 Radar data

For this study, data from Nîmes and Collobrières S-band polarimetric radars, indicated by gray stars in Figure 2, are used. A polarimetric processing chain has been implemented on these radars (Figueras i Ventura et al. (2012); Figueras i Ventura and Tabary (2013)) and provides the horizontal reflectivity Z_{hh} , the differential reflectivity Z_{dr} (corrected and non-corrected from attenuation), the differential phase ϕ_{dp} , the specific differential phase K_{dp} and the co-polar correlation coefficient ρ_{hv} at a $240 \text{ m} \times 0.5^\circ$ resolution with a maximum range of 255 km. An hydrometeor classification by a fuzzy logic algorithm (Al-Sakka et al., 2013) was applied to the polarimetric data. The hydrometeor are classified into the following categories: rain, wet-snow, dry-snow, hail and pristine ice. An illustration of the classification is shown in Figure 3 for Nîmes radar on 24 September 2012 at 0300 UTC for elevation 0.6° . The corresponding polarimetric variables are shown in section 4.1.

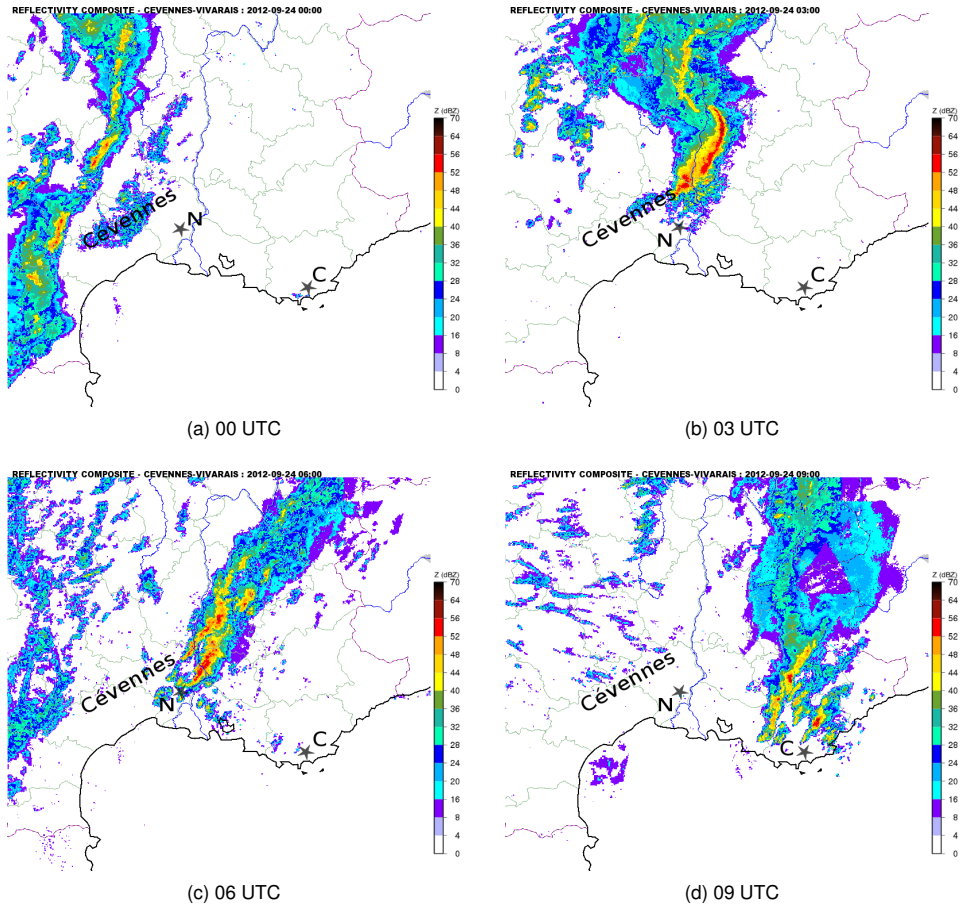


Figure 2: Radar reflectivity mosaic observed at 00, 03, 06 and 09 UTC on 24 September 2012 in south-east France. Nimes and Collobrières S-band radars are indicated by gray stars and by the letters N and C respectively.

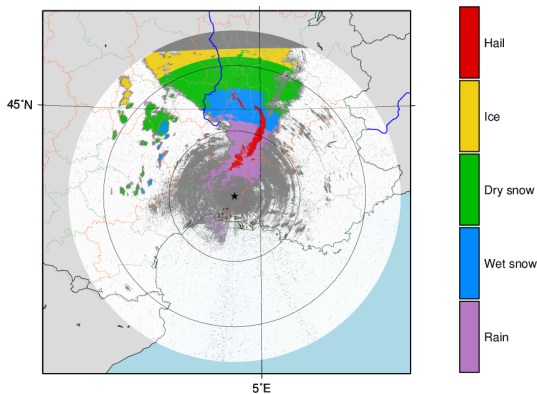


Figure 3: Hydrometeor classification for Nimes radar on 24 September 2012 at 0300 UTC. Elevation 0.6° . The gray color indicates non-meteorological echoes.

Data are available for six elevation angles every 5 min. Only the lower-elevation angles (below 3°) are repeated every 5 min and a few higher-elevation angles are added in order to form a complete volume in a “su-

percycle” of 15 min.

3.3 Simulated data

The simulation is performed with Meso-NH model at a 2.5 km horizontal resolution. The simulation is initialized and coupled with AROME WMed NWP model. It is a special version of AROME operational model that was developed for the HyMeX campaign with a domain covering the western Mediterranean. Different sensitivity tests (initialization time, transport numerical scheme) have been carried out in order to choose the best configuration of Meso-NH compared to the observations. These tests are described in detail by Kaufmann (2013).

The initialization of the simulation starts on 24 September 2012 at 00 UTC. The polarimetric simulator is applied to the output of the Meso-NH simulation and the polarimetric variables are then calculated on the same polar grid than the radar ($240 \text{ m} \times 0.5^\circ$) for all elevation angles scanned by the radar.

4 RESULTS

4.1 Subjective comparison between observed and simulated polarimetric variables

In this section, individual Plan Position Indicators (PPIs) of observed and simulated polarimetric variables (Z_{hh} , Z_{dr} , K_{dp} , ϕ_{dp} , ρ_{hv}) are compared for Nîmes radar on 24 September 2012 at 0300 UTC. For simulated variables, the attenuation is not taken into account while the observed Z_{hh} and Z_{dr} are corrected from attenuation (only in rain) with the following formulas (Figueras i Ventura et al., 2012):

$$Z_{hh_{corr}} = Z_{hh} + 0.04 * \phi_{dp}$$

$$Z_{dr_{corr}} = Z_{dr} + 0.004 * \phi_{dp}$$

The convective line is rather well captured by the model in the reflectivity field Z_{hh} (Figure 4). However the position of the simulated convective line is shifted north-westwards compared to the observed line and the model slightly underestimates the maximum values of reflectivity. This can be explained by the fact that the maximum radar reflectivities are due to hail, which was observed at

ground and is identified by the classification (shown in red in Figure 3), whereas the model can't represent hail. The simulated values of differential reflectivity Z_{dr} are of the same order as the observed ones, but less negative values of Z_{dr} are simulated than observed. Because attenuation is particularly strong for this case for an S-band radar, as can be inferred from the differential phase field ϕ_{dp} shown in Figure 5, we suspect that the observed negative Z_{dr} values could be partly due to an insufficient attenuation correction in radar data. No attenuation is indeed corrected in wet snow for example although it could be significant. K_{dp} maximum values are slightly underestimated in the simulation, which may be linked to the underestimation of the maximum reflectivity values.

Observed ρ_{hv} values are clearly lower than the simulated values (Figure 6), with a majority of the values below 0.98 whereas the simulated ρ_{hv} values are comprised between 0.99 and 1 everywhere. The observed ρ_{hv} values are particularly low in the area suffering from strong attenuation (north-east of Nîmes radar). This is consistent with the results of Ryzhkov (2007), who showed noticeable decreased of ρ_{hv} in areas with large cross-beam gradients. However observed ρ_{hv} values are slightly higher on Collobrières radar, with more values between 0.99 and 1.

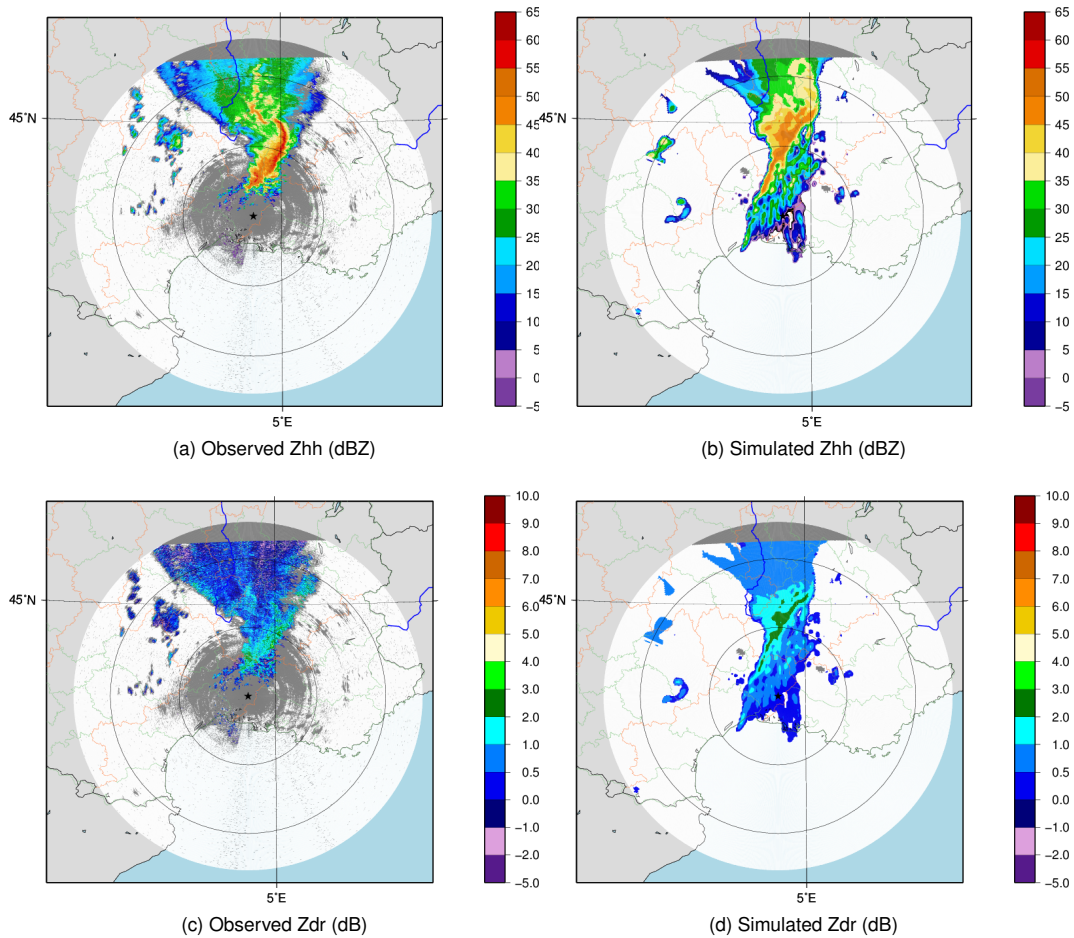


Figure 4: Observed and simulated reflectivity (Zhh) and differential reflectivity (Zdr). Nimes radar on 24 September 2012 at 0300 UTC. Elevation 0.6° . The gray circles indicate distances of 100 km and 200 km from the radar. For radar and model images, all pixels with a reflectivity value below noise level are in white. The gray color indicates non-meteorological echoes for radar images while it represents data outside model domain for model images.

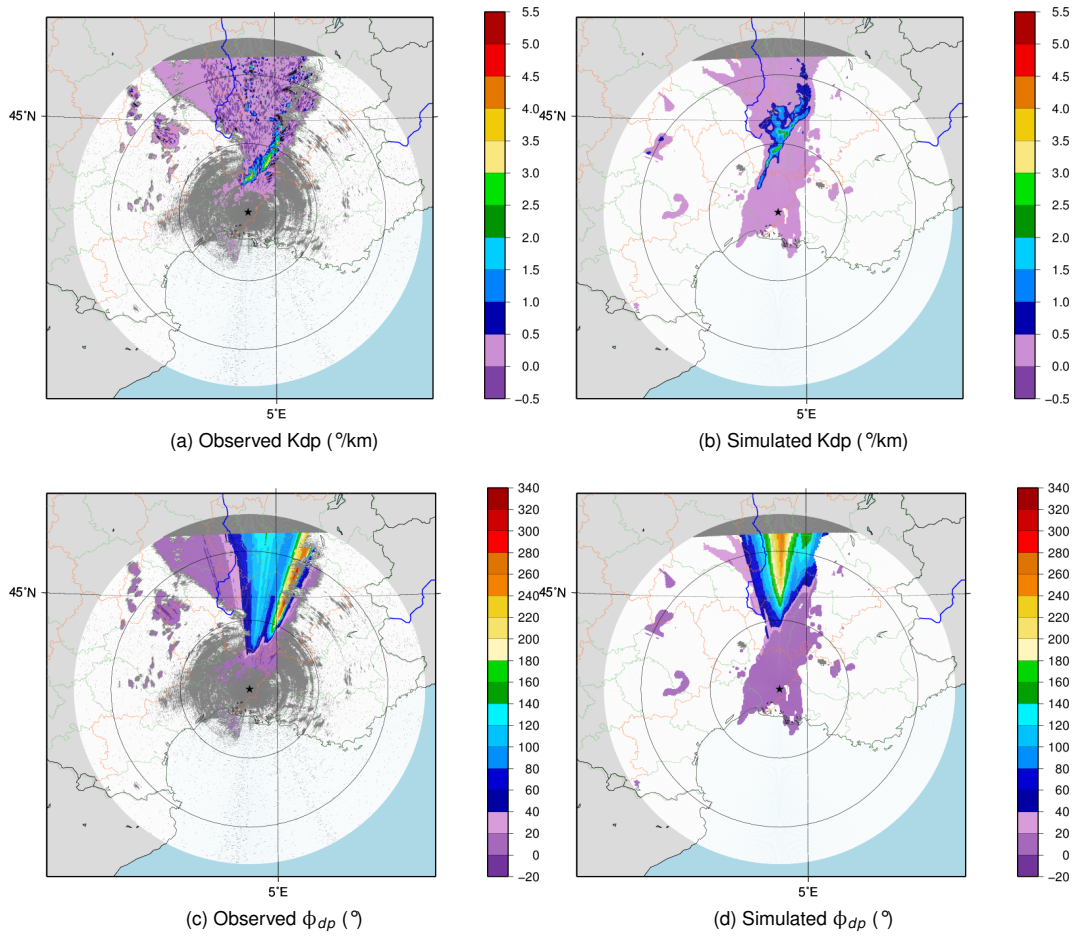


Figure 5: Same as Figure 4 but for specific differential phase (K_{dp}) and differential phase ϕ_{dp} .

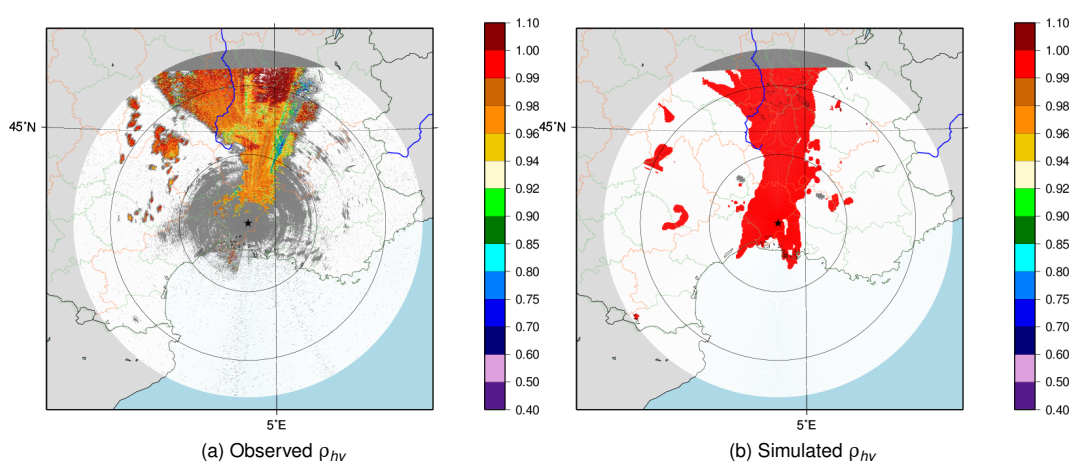


Figure 6: Same as Figure 4 but for co-polar correlation coefficient ρ_{hv} .

4.2 Distributions of polarimetric variables as a function of temperature

In order to overcome problems of time-space lags between model and radar data, integrated distributions of simulated and observed polarimetric variables as a function of model temperature are studied. Vertical profiles of Zhh, Zdr, Kdp and ρ_{hv} were created by integrating their values for all elevation angles from 00 to 12 UTC on 24 September 2012, every 15 minutes, i.e. for 52 full radar volumes. For these statistics, non-meteorological echoes identified by the classification algorithm, as well as pixels below noise level and pixels with a partial beam blockage over 10% were removed. To avoid too large a spread of the pixels in terms of horizontal distance, only the pixels between 80 and 100 km from the radar were selected. Furthermore, the profiles were created in convective areas only. To select convective areas, the following method was applied: for a given "vertical" combination of pixels defined by one range and one azimuth (and all elevation angles available), the "column" was considered as convective only if all elevations with a temperature over 5°C had a reflectivity over 45 dBZ.

The profiles of observed and simulated horizontal re-

flectivity are shown in Figure 7. The profiles have overall the same shape with (by construction) values over 45 dBZ for temperatures over 5°C and a decrease of the reflectivities with altitude. However, for temperatures below -5°C, the decrease of observed Zhh values is significantly more important than for simulated Zhh. This could be partly explained by an insufficient attenuation correction, in particular because no attenuation is corrected in wet snow, although it could be significant. Attenuation correction factors in snow and wet snow are currently being investigated (see poster 369 by A. Boumahmoud and presentation 7B.2 by H. Al-Sakka).

Another difference between radar and model profiles is the clear "step" formed by the sudden decrease of reflectivity for temperature below 0°C in the model whereas the decrease is more continuous for radar reflectivities. This can be explained by the abrupt distinction between liquid and ice particles in the model. In this first version of the polarimetric radar simulator, no continuous melting model was indeed implemented. The only hydrometeor that contains ice and liquid water at the same time is graupel but the transition is abrupt at 0°C: graupel particles are made of ice only for temperatures below 0°C and contain 14% of liquid water for temperatures over 0°C.

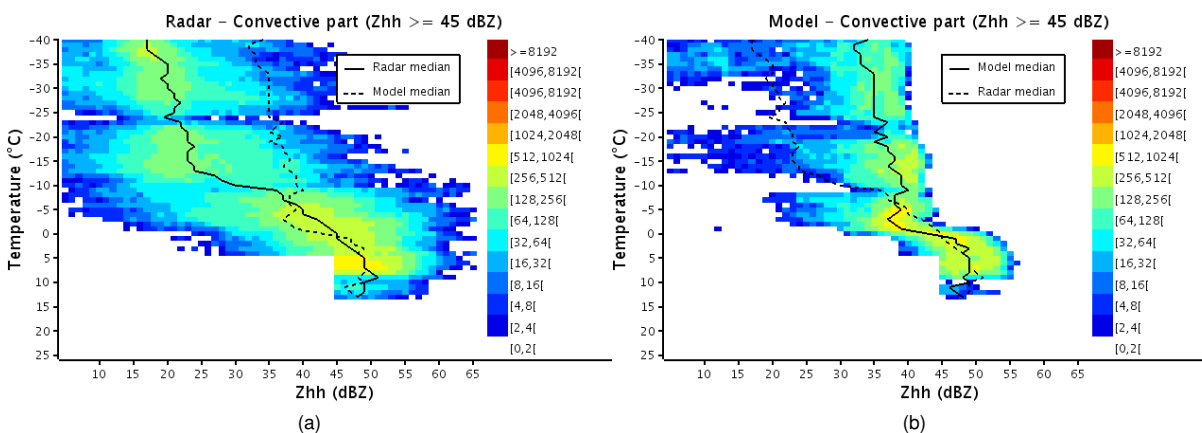


Figure 7: Distribution of observed (a) and simulated (b) Zhh in convective areas as a function of model temperature from 00 to 12 UTC on 24 September 2012 for Nîmes radar. The median for simulated (model) and observed (radar) data are indicated in black.

Profiles of Zdr in convective areas are presented in Figure 8 (a) and (b). Although simulated and observed Zdr profiles have overall the same shape (i. e. a decrease of Zdr with decreasing temperatures until about 0°C and constant values for temperatures lower than 0°C), the median observed Zdr is about 1 dB lower than the median simulated Zdr (for positive temperatures) and about 1.5 dB lower for negative temperatures. The same profile was

calculated for Collobrieres radar (for the same event), and about the same difference was observed. The radar profile is probably too low because it shows negative median values of Zdr for temperatures below 2°C, which would indicate that a large part of the hydrometeors in temperature regions below 2°C have prolate shapes. An insufficient attenuation correction on Zdr could partly explain these negative values, as well as a calibration bias. For

simulated Zdr, the same sudden decrease as observed for simulated Zhh can be seen around 0°C. Like for Zhh, this is probably due to the dependency of Zdr to the dielectric factor and to the fact that the distinction between liquid and ice particles in the model is abrupt.

Observed and simulated Kdp profiles (Figure 8 (c) and (d)) are more consistent. Like for Zdr, Kdp values decrease with altitude, showing that oblate particles have more weight in low levels (in convective rain) than in altitude (snow, graupel, ice). Simulated Kdp is slightly higher than observed Kdp (of about 0.4°/km). On the contrary to Zdr, Kdp is not affected by attenuation or by radar bias.

This difference could be explained by an uncorrect parameterization in the polarimetric simulator. The parameterized oblateness of snow and graupel particles (0.75) may be too strong? Or this can also be due to the higher values of simulated Zhh in altitude. Sensitivity studies to the axis ratio of hydrometeors will have to be carried out to retrieve the values that best match with the observations. This difference could also be due to an underestimation of observed Kdp, because it is estimated based on 25 range gates linear regression over ϕ_{dp} which is also filtered (Figuera i Ventura et al., 2012).

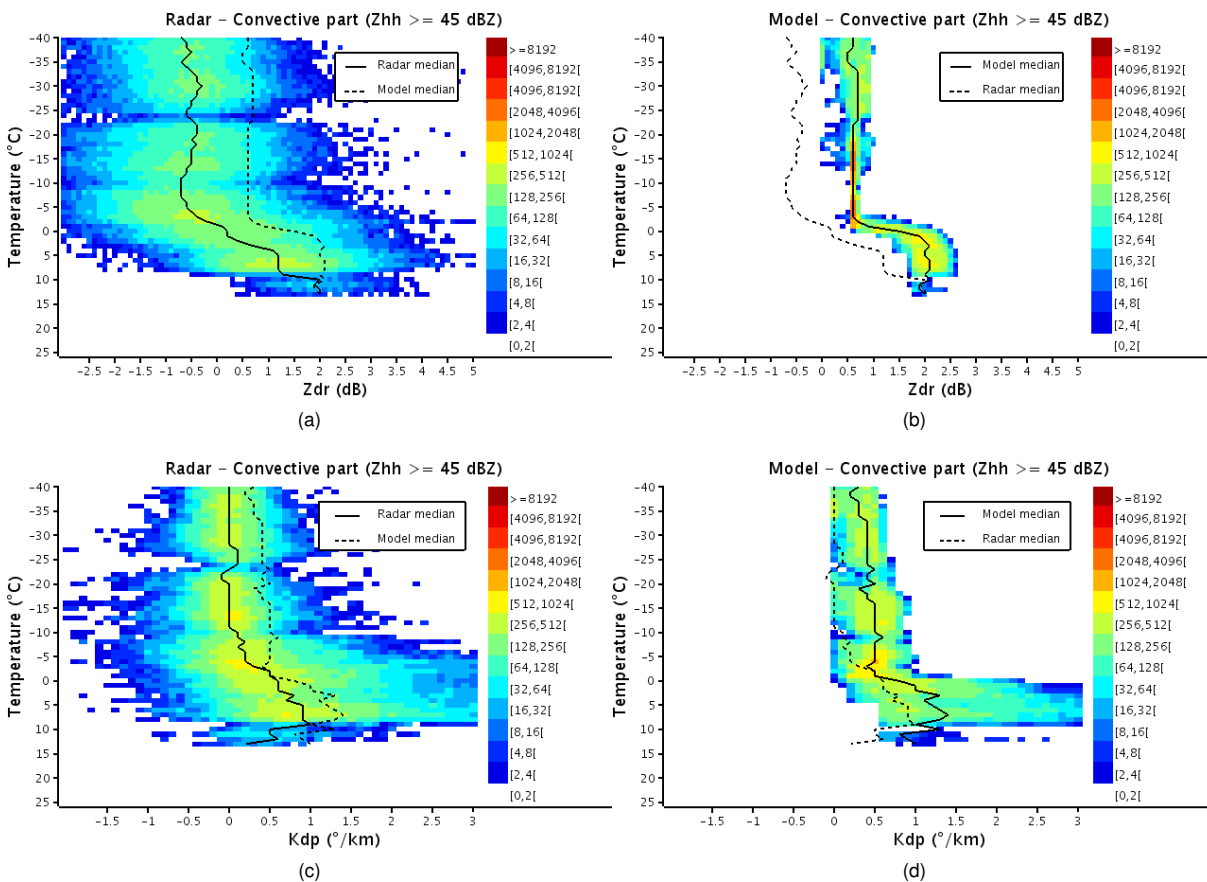


Figure 8: Distribution of observed (a), (c) and simulated (b), (d) Zdr (a), (b) and Kdp (b), (c) in convective areas as a function of model temperature from 00 to 12 UTC on 24 September 2012 for Nîmes radar.

Profiles of observed and simulated ρ_{hv} in convective areas are shown in Figure 9. All model values are between 0.99 and 1.1 whereas radar values are very scattered. The median radar ρ_{hv} is mainly around 0.96 whereas the median model ρ_{hv} is 0.99. But ρ_{hv} coefficient is particularly low for Nîmes radar. A median of 0.98 was observed for Collobrières S-band radar. Differ-

ent reasons can explain why the observed ρ_{hv} is lower than the simulated ρ_{hv} . First, measurement noise is not taken into account in the model and contributes to decrease ρ_{hv} . Moreover, graupel and snow particles are simulated as spheroids whereas they can have more irregular shapes in reality and this leads to an overestimation of ρ_{hv} in the model. Balakrishnan and Zrnic (1990)

found that increasing canting angle and liquid water fraction in melting species contributes to decrease ρ_{hv} . Adjusting these parameters in our simulator could also help

reduce the difference between observed and simulated values.

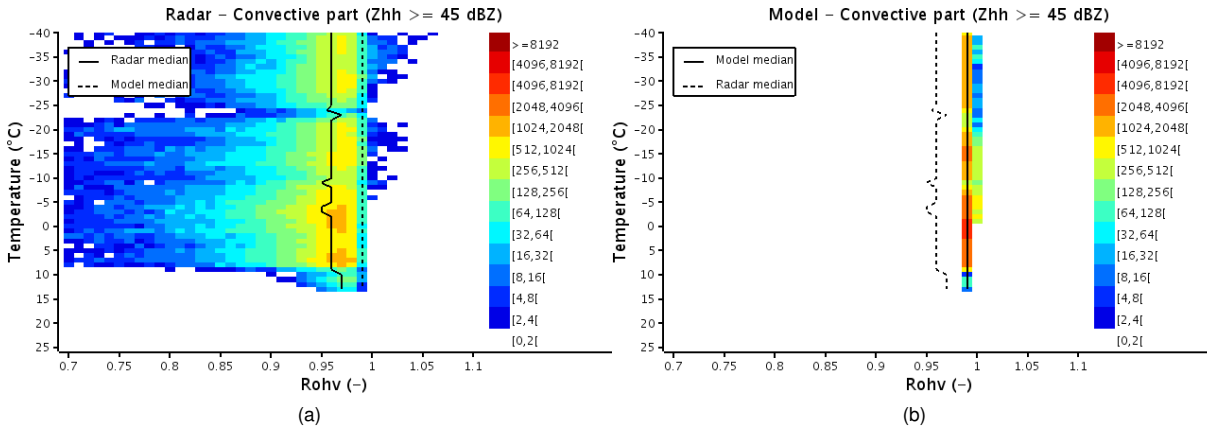


Figure 9: Distribution of observed (a) and simulated (b) ρ_{hv} in convective areas as a function of model temperature from 00 to 12 UTC on 24 September 2012 for Nîmes radar.

4.3 Polarimetric variables as a function of horizontal reflectivity for each hydrometeor class

In this section, the distribution of observed and simulated Zdr and Kdp as a function of horizontal reflectivity are compared. Like in the previous section, the distributions were created by integrating the polarimetric variables for all elevation angles from 00 to 12 UTC on 24 September 2012. For these statistics, non-meteorological echoes identified by the classification algorithm, as well as pixels below noise level and pixels with a partial beam blockage over 10% were removed. Furthermore, to avoid attenuation problems, pixels with a differential phase greater than 10° were also removed.

For simulated data the distributions of Zdr and Kdp are shown for rain, snow and graupel (for temperatures

greater than 0°C). They are compared to radar data for rain, dry snow and wet snow hydrometeor classes. The correspondence between model and radar classes is not perfect. The radar and model "rain" class should fairly well represent the same particles. Because snow particles are considered to be made of ice and air only in the model, the model "snow" class should also be rather equivalent to the radar "dry snow" class. However, the model "graupel" category (for positive temperatures) is compared to the "wet snow" radar class because it is the only model category that contains liquid water and ice at the same time. But it does not necessarily represent the same particles. The "wet snow" radar class probably contains more water than the graupel model class, in which the particles have a fixed water fraction of 14%.

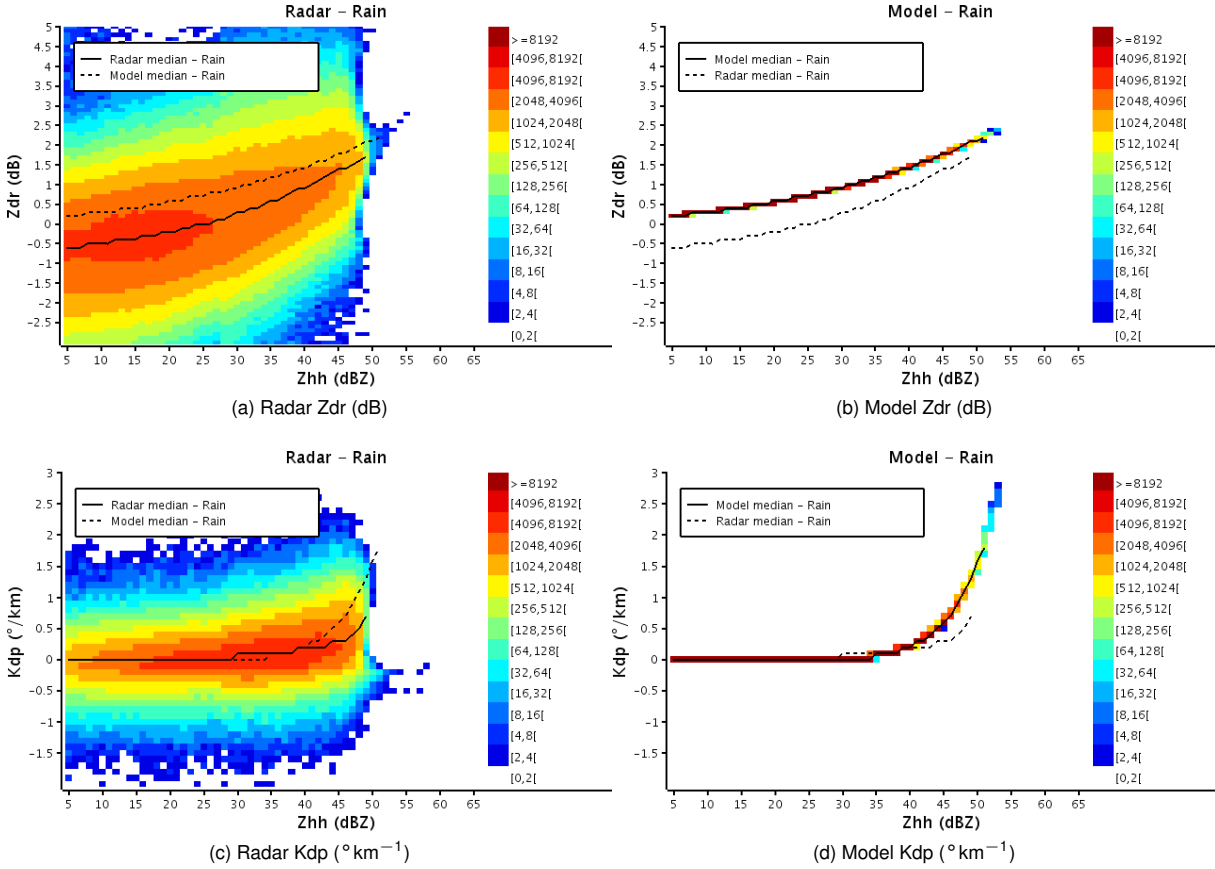


Figure 10: Observed and simulated differential reflectivity (Zdr) and specific differential phase (Kdp) as a function of reflectivity (Zhh) for rain.

Zdr and Kdp distributions are shown in Figure 10 for rain. The most striking difference between radar and model distributions is the fact that observed Zdr and Kdp values for a given Zhh are very scattered whereas simulated Zdr and Kdp are almost completely determined by Zhh. The very low dispersion in simulated data can be explained first by the fact that radar measurement noise is not simulated and second because Meso-NH model uses a one-moment bulk microphysical scheme, which gives only one degree of liberty: for a given Zhh, Zdr in rain depends on temperature only. A difference of about 0.6 dB can be observed between radar and model Zdr medians. Radar Zdr is necessarily negatively biased because for reflectivities below 25 dBZ, the median radar Zdr is negative which would indicate prolate rain particles. However, if one refers to Tabary et al. (2011), Zdr should be around 0.2 for Zhh values between 20 and 22 dBZ. This is also not the case for simulated Zdr, which is more around 0.5 dB. The comparison between these observed and simulated Zdr value as a function of Zhh shows therefore that at the same time the observed Zdr in rain seems negatively biased and the simulated Zdr seems slightly over-

estimated.

Observed and simulated Kdp profiles as a function of Zhh, shown in Figure 10 (c) and (d), are more consistent with each other, although radar data are again significantly more scattered. For reflectivity values until 40 dBZ, radar and model profiles are very close, but from 40 dBZ simulated Kdp increases more strongly than observed Kdp. As Kdp is not affected by attenuation, we can't explain this difference by an underestimation of radar Kdp. This could be due to an overestimation of the oblateness of the particles in the model but for rain, the formula chosen from Brandes et al. (2002) seems widely acknowledged. But Kdp also strongly depends on the drop size distribution $N(D)$ (Bringi and Chandrasekar, 2001), and the overestimation of Kdp in the simulation could be explained by an inappropriate parameterization of $N(D)$ in the polarimetric simulator. However, like mentioned for Figure 8, the observed Kdp is also probably underestimated because of its estimation method based on 25 range gates linear regression over ϕ_{dp} . New algorithms for Kdp estimation will have to be studied in order to avoid underestimating it.

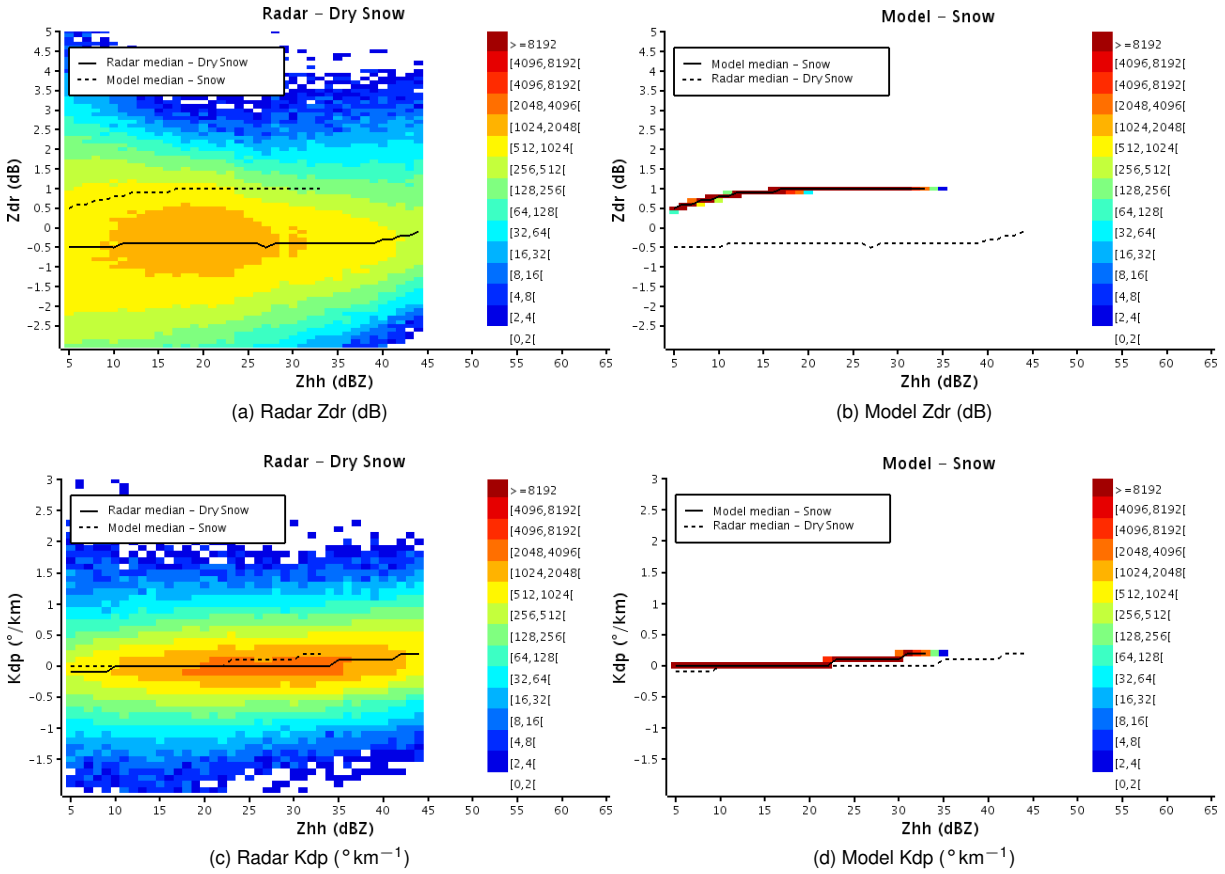


Figure 11: Observed and simulated differential reflectivity (Z_{dr}) and specific differential phase (K_{dp}) as a function of reflectivity (Z_{hh}) for dry snow.

In snow (Figure 11, simulated and observed Z_{dr} are both almost constant with Z_{hh} , although simulated Z_{dr} slightly increases (by 0.5°) from 5 to 20 dBZ. This slight increase may be due to the increase of ice content with Z_{hh} . This figure confirms the choice of taking a constant axis ratio function for snow. However the median simulated Z_{dr} is 1.5 dB higher than the median observed Z_{dr} . Even if we suppose that radar Z_{dr} is, like for rain, biased

by about 0.5 dB, the simulated Z_{dr} would still be too high by 1 dB. Our axis ratio function (0.75) may be too low for snow particles.

Observed and simulated distributions of K_{dp} as a function of Z_{hh} are very close. Both slightly increase with Z_{hh} . Simulated K_{dp} increases slightly more strongly which confirms a too low value for the snow particles axis ratio.

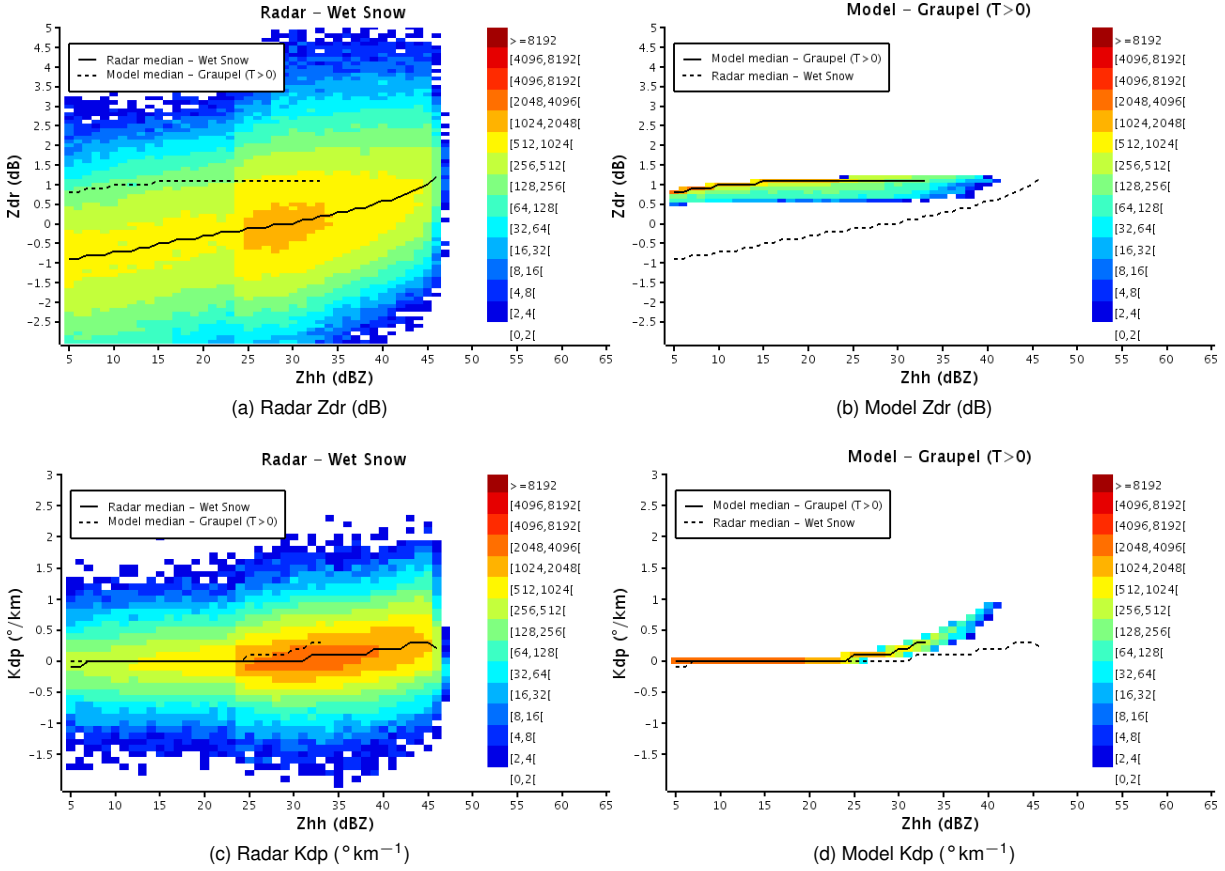


Figure 12: Observed and simulated differential reflectivity (Zdr) and specific differential phase (Kdp) as a function of reflectivity (Zhh) for wet snow or graupel.

Observed and simulated member functions for radar "wet snow" and model graupel (Figure 12) are more different. This is partly due to the fact that, as mentioned previously, the graupel category in the model does not represent exactly the same particles as the radar "wet snow" class. Observed Zdr increases clearly more strongly with Zhh than the simulated Zdr. This can probably be explained by the fact that Zdr strongly depends on the dielectric function and that "wet snow" particles may contain more and more water with the increase of Zhh, whereas the water fraction for graupel particles below melting level is fixed to 14%.

On the contrary, simulated Kdp increases more strongly than the observed Kdp. This could be attributed to too low an axis ratio (0.75) in the model or to an underestimation of observed Kdp.

5 DISCUSSION AND CONCLUSION

A polarimetric radar simulator has been developed within Meso-NH model, in order to enable direct comparisons

between measured dual-pol data and numerically modeled data. The simulator takes as input the output of model simulations such as hydrometeor contents (rain, snow and graupel and ice), temperature, and ice concentration. The following polarimetric variables are simulated: reflectivity (Zhh), differential reflectivity (Zdr), differential phase (ϕ_{dp}), specific differential phase (Kdp) and copolar cross-correlation coefficient (ρ_{hv}). Within the simulator, pristine ice particles are considered to be spherical whereas rain, snow and graupel particles are simulated as spheroids.

Observed and simulated polarimetric variables were compared for the bow echo case on 24 September 2012, for Nîmes and Collobrières S-band radars. Subjective comparisons were first conducted by comparing individual observed and simulated PPIs. Statistic comparisons were then performed by comparing distributions of Zhh, Zdr, Kdp and ρ_{hv} as a function of temperature (in convective areas), integrated from 00 to 12 UTC on 24 September 2012. Distributions of observed and simulated Zdr and Kdp as a function of Zhh were also compared for

three hydrometeor categories.

Different conclusions can be drawn from these comparisons. First, simulated data are clearly less scattered than observations, which is probably mainly because radar noise is not simulated in the model, and also because of the one-moment microphysical scheme used by Meso-NH. Work is currently underway to implement a two-moment scheme within Meso-NH model and comparisons between simulated polarimetric variables with one and two moment schemes should be soon possible. The differences in scatter between model and radar data could also be partly due to the different horizontal resolution between simulated data ($2.5\text{ km} \times 2.5\text{ km}$) and radar data ($240\text{ m} \times 0.5^\circ$). Simulations at higher resolution could be performed in the future, in order to test the impact of model resolution on simulated polarimetric variables.

These comparisons have also shown a significant bias in radar Zhh (in comparison with model Zhh), for temperatures below 0°C . This bias could be due to an overestimation of the hydrometeor contents in altitude by the model, leading to an overestimation of reflectivity. But the lower observed Zhh is also suspected to be partly due to an insufficient attenuation correction, in particular because attenuation is corrected for rain only whereas it could be significant for other species also, in particular for wet snow (which corresponds to the melting layer). Work is currently underway to calculate attenuation correction factors in wet snow and snow (see poster 369 by A. Boumahmoud and presentation 7B.2 by H. Al-Sakka). Radar Zdr is also clearly biased but this is probably a calibration bias.

The comparison of distributions of observed/simulated Zdr and Kdp as a function of Zhh (for pixels with no attenuation) have also shown that for rain and for snow, simulated Kdp increases more strongly with Zhh than observed Kdp. This could be due to an underestimation of observed Kdp because of its estimation method from ϕ_{dp} . To evaluate the possible underestimation of Kdp during its estimation method, the "intrinsic" model Kdp could be compared to a Kdp calculated from simulated ϕ_{dp} with the same method as is applied to raw radar data. For dry snow, observed Zdr is almost constant with Zhh, which shows that the choice of taking a constant axis ratio is reasonable. The comparison between radar "wet snow" category and model "graupel for temperatures higher than 0°C " category highlights the difficulty of comparing radar and model categories, which do not represent exactly the same particles. It also shows that adding a melting model in the simulator, such as described by Jung et al. (2008), could be useful to better simulate "wet snow".

Different sensitivity tests are planned to be conducted in the near future. The sensitivity of polarimetric variables to particle axis ratio and also to canting angle will be in-

vestigated. The main objective is to best adjust these parameters in order to minimize the differences between radar and model observables. Comparisons with X and C-band radars will also be carried out for this case, and other cases will also be studied. The final aim of this study is to assess how and in which conditions the polarimetric variables could be used for data assimilation in NWP models.

6 ACKNOWLEDGEMENTS

The help of A. Boumahmoud, H. Al-Sakka, B. Fradon from Météo France Radar Center, and also of J. F. Ribaud, G. Kaufmann, C. Lac and E. Chabot from Météo France CNRM is greatly acknowledged.

REFERENCES

- Al-Sakka, H., A.-A. Boumahmoud, B. Fradon, S. J. Frasier, and P. Tabary, 2013: A new fuzzy logic hydrometeor classification scheme applied to the french x, c and s-band polarimetric radars. *Journal of Applied Meteorology and Climatology*.
URL <http://journals.ametsoc.org/doi/abs/10.1175/JAMC-D-12-0236.1>
- Balakrishnan, N. and D. Zrnic, 1990: Use of polarization to characterize precipitation and discriminate large hail. *Journal of the atmospheric sciences*, **47**, 1525–1540.
URL <http://repository.ias.ac.in/1034/>
- Bohren, C. F. and L. J. Battan, 1982: Radar backscattering of microwaves by spongy ice spheres. *Journal of the Atmospheric Sciences*, **39**, 2623–2628.
URL [http://journals.ametsoc.org/doi/abs/10.1175/1520-0469\(1982\)039%3C2623%3ARBOMBS%3E2.0.CO%3B2](http://journals.ametsoc.org/doi/abs/10.1175/1520-0469(1982)039%3C2623%3ARBOMBS%3E2.0.CO%3B2)
- Brandes, E. A., G. Zhang, and J. Vivekanandan, 2002: Experiments in rainfall estimation with a polarimetric radar in a subtropical environment. *Journal of Applied Meteorology*, **41**, 674–685.
URL [http://journals.ametsoc.org/doi/abs/10.1175/1520-0450\(2002\)041%3C0674:EIREWA%3E2.0.CO;2](http://journals.ametsoc.org/doi/abs/10.1175/1520-0450(2002)041%3C0674:EIREWA%3E2.0.CO;2)
- Bringi, V. and V. Chandrasekar, 2001: *Polarimetric Doppler weather radar: principles and applications*. Cambridge University Press.
- Caumont, O., V. Ducrocq, G. Delrieu, M. Gosset, J.-P. Pinty, J. Parent du Châtelet, H. Andrieu, Y. Lemaître, and G. Scialom, 2006: A radar simulator for high-resolution nonhydrostatic models. *Journal of Atmospheric and Oceanic Technology*, **23**, 1049–1067.
URL <http://journals.ametsoc.org/doi/abs/10.1175/JTECH1905.1>

- Caumont, O., V. Ducrocq, É. Wattrelot, G. Jaubert, and S. PRADIER-VABRE, 2010: 1d+ 3dvar assimilation of radar reflectivity data: a proof of concept. *Tellus A*, **62**, 173–187.
- Drobinsky, 2013: Hymex, a 10-year multidisciplinary program on the mediterranean water cycle, submitted to BAMS.
- Ducrocq, V., 2013: Hymex-sop1, the field campaign dedicated to heavy precipitation and flash flooding in the northwestern mediterranean, submitted to BAMS.
- Figueras i Ventura, J., A.-A. Boumahmoud, B. Fradon, P. Dupuy, and P. Tabary, 2012: Long-term monitoring of french polarimetric radar data quality and evaluation of several polarimetric quantitative precipitation estimators in ideal conditions for operational implementation at c-band. *Quarterly Journal of the Royal Meteorological Society*, **138**, 2212–2228.
URL <http://onlinelibrary.wiley.com/doi/10.1002/qj.1934/full>
- Figueras i Ventura, J. and P. Tabary, 2013: The new french operational polarimetric radar rainfall rate product. *Journal of Applied Meteorology and Climatology*.
URL <http://journals.ametsoc.org/doi/abs/10.1175/JAMC-D-12-0179.1>
- Hufford, G., 1991: A model for the complex permittivity of ice at frequencies below 1 thz. *International Journal of Infrared and Millimeter Waves*, **12**, 677–682.
URL <http://link.springer.com/article/10.1007/BF01008898>
- Jung, Y., G. Zhang, and M. Xue, 2008: Assimilation of simulated polarimetric radar data for a convective storm using the ensemble kalman filter. part i: Observation operators for reflectivity and polarimetric variables. *Monthly Weather Review*, **136**, 2228–2245.
URL <http://journals.ametsoc.org/doi/pdf/10.1175/2007MWR2083.1>
- Kabeche, F., J. F. i Ventura, B. Fradon, A.-A. Boumahmoud, S. Frasier, and P. Tabary, 2012: Design and test of an x-band optimal rain rate estimator in the frame of the rhytmme project. *Proc. European Conf. on Radar in Meteorology and Hydrology, ERAD 2012*.
- Kaufmann, G., 2013: *Evaluation de schémas micro-physiques sur des systèmes convectifs profonds*. Master's thesis, Ecole Nationale de la Météorologie.
- Lafore, J. P., J. Stein, N. Asencio, P. Bougeault, V. Ducrocq, J. Duron, C. Fischer, P. Hérelil, P. Mascart, V. Masson, and et al., 1998: The meso-nh atmospheric simulation system. part i: adiabatic formulation and control simulations. *Annales Geophysicae*, **16**, 90–109, doi:10.1007/s00585-997-0090-6.
URL <http://dx.doi.org/10.1007/s00585-997-0090-6>
- Liebe, H. J., G. A. Hufford, and T. Manabe, 1991: A model for the complex permittivity of water at frequencies below 1 thz. *International Journal of Infrared and Millimeter Waves*, **12**, 659–675.
URL <http://link.springer.com/article/10.1007/BF01008897>
- Mishchenko, M. I. and L. D. Travis, 1994: T-matrix computations of light scattering by large spheroidal particles. *Optics communications*, **109**, 16–21.
URL <http://www.sciencedirect.com/science/article/pii/0030401894907315>
- Montmerle, T. and C. Faccani, 2009: Mesoscale assimilation of radial velocities from doppler radars in a preoperational framework. *Monthly Weather Review*, **137**, 1939–1953.
URL <http://journals.ametsoc.org/doi/abs/10.1175/2008MWR2725.1>
- Pfeifer, M., G. Craig, M. Hagen, and C. Keil, 2008: A polarimetric radar forward operator for model evaluation. *Journal of Applied Meteorology and Climatology*, **47**, 3202–3220.
URL <http://journals.ametsoc.org/doi/abs/10.1175/2008JAMC1793.1>
- Pinty, J.-P. and P. Jabouille, 1998: A mixed-phased cloud parameterization for use in a mesoscale non-hydrostatic model: Simulations of a squall line and of orographic precipitation. *Proc. Conf. on Cloud Physics, Everett, WA, Amer. Meteor. Soc.*
- Ryzhkov, A., M. Pinsky, A. Pokrovsky, and A. Khain, 2011: Polarimetric radar observation operator for a cloud model with spectral microphysics. *Journal of Applied Meteorology and Climatology*, **50**, 873–894, doi:10.1175/2010JAMC2363.1.
URL <http://dx.doi.org/10.1175/2010JAMC2363.1>
- Ryzhkov, A. V., 2007: The impact of beam broadening on the quality of radar polarimetric data. *Journal of Atmospheric and Oceanic Technology*, **24**, 729–744.
URL <http://journals.ametsoc.org/doi/abs/10.1175/JTECH2003.1>
- Seity, Y., P. Brousseau, S. Malardel, G. Hello, P. Bénard, F. Bouttier, C. Lac, and V. Masson, 2011: The arôme-france convective-scale operational model. *Monthly Weather Review*, **139**, 976–991.
URL <http://journals.ametsoc.org/doi/abs/10.1175/2010MWR3425.1>
- Tabary, P., A.-A. Boumahmoud, H. Andrieu, R. J. Thompson, A. J. Illingworth, E. L. Bouar, and J. Testud, 2011: Evaluation of two integrated polarimetric quantitative precipitation estimation (qpe) algorithms at c-band. *Journal of Hydrology*, **405**, 248–260.
URL <http://www.sciencedirect.com/science/article/pii/S0022169411003313>